Contactless surface flattening of additive manufactured nickel-base alloy parts by ultra-short pulsed laser ablation

Author(s):
Weixler, Jodok; Gerstgrasser, Marcel; Wegener, Konrad

Publication date:
2020

Permanent link:
https://doi.org/10.3929/ethz-b-000462589

Originally published in:
Procedia CIRP 95, https://doi.org/10.1016/j.procir.2020.01.142

Available online at www.sciencedirect.com

ScienceDirect

Procedia CIRP 95 (2020) 933–937

www.elsevier.com/locate/procedia

20th CIRP CONFERENCE ON ELECTRO PHYSICAL AND CHEMICAL MACHINING

Contactless surface flattening of additive manufactured nickel-base alloy parts by ultra-short pulsed laser ablation

J. Weixler *[a], M. Gerstgrasser [a], K. Wegener [a]

[a]*Institute of Machine Tools and Manufacturing, ETH Zürich, Leonhardstrasse 21, 8092 Zürich, Switzerland*

* Corresponding author. Tel.: +41 44 633 79 86; fax: +41 44 633 14 92. *E-mail address:* weixler@iwf.mavt.ethz.ch

Abstract

Nickel-base alloy samples produced by selective laser melting (SLM) exhibit high surface roughness of 14.2 µm ± 4.8 µm standard deviation at the sidewalls. Ultra-short pulsed (USP) laser ablation at a pulse duration of 10 ps is applied to reduce the surface roughness. This flattening method does not require a melting phase. The influence of the tilt angle and the orientation of the SLM layers on the surface topography of the sample is investigated. Orthogonal laser ablation of Ni-base alloy samples leads to irregular surface topography and exposure of sharp spikes. Surface flattening by laser ablation is demonstrated applying a tilt angle of 80° in combination with a projected pulse fluence of 0.21 J cm^{-2}. A significant influence of the tilt angle and SLM layer orientation on the surface roughness is observed.

Keywords: Ultra short-pulsed laser ablation; surface flattening; laser flattening; Nd:YAG; CM247LC; Ni-base alloy; post-treatment selective laser melting;

1. Introduction

Additive manufacturing (AM) is a manufacturing technology, which enables the production of very complex geometries, which cannot be produced by conventional machining techniques. Additionally, a high degree of customization of products is enabled by AM. However, for the most cases, the surface quality after AM processing does not meet the requirements of the final application, which makes post-treatment necessary.

Mechanical processing such as milling or turning are a suitable technique for post-treatment enabling high removal rates. However, mechanical processing requires clamping, the mechanical loads as well as vibration and the accessibility can be limiting factors.

Electrical discharge machining is a possible post-treatment approach as well but can cause phase transformation due to the residual heat in the work piece. For post-processing of features with high aspect ratio such as small holes and tiny valleys, the aforementioned post-processing techniques are limited in terms of accessibility.

Post-treatment by laser is very flexible in terms of deflection speed and local surface modification. High laser scan speeds are achieved by scanning optics. The process forces in laser treatment are very small and can be neglected on the part scale. USP laser ablation in particular enables removal of material independent of the material strength. The short interaction time of the laser pulse with high intensity induces very effective material removal, and heat conduction into the bulk material is minimized [1].

Ni-base alloys are predestinated material designed for directionally solidified parts, which have to withstand high temperature and high stress conditions such as turbine blades in a jet engine [2-4]. Turbine blades conventionally are manufactured by casting. Costs for casting tools are high and different variants of turbine blades require different casting tools. SLM processing offers a high geometrical flexibility and no tool is necessary. Therefore, it has the potential to

10.1016/j.procir.2020.01.142

replace casting as a manufacturing technique for turbine blades [5].

High-pressure turbine blades require film cooling realized by a large number of holes on the surface [6]. The cooling effectiveness for film cooling is very sensitive to the surface roughness in the hole. Snyder et al. investigated the potential of controlling the surface roughness by manipulation of the laser parameters [7]. However, the surface topography resulting from SLM processing is not sufficient and requires post-treatment.

Solheid et al. [8] performed laser polishing of additive manufactured 18-Ni 300 grade samples using a continuous wave and 200 ns pulsed laser source. The polishing mechanism is dominated by re-melting, therefore high surface temperatures are present in the processing area. Phase transformation and formation of cracks is observed after laser polishing for all cases. The initial surface roughness of Ra= 6.4 µm was reduced down to Ra= 0.6 µm.

The potential of reducing the surface roughness on stainless steel using USP laser has been studied by Romoli [9]. The initial roughness Sa = 200 nm is reduced by as factor of two down to Sa=100 nm. High surface quality is achieved by Timmer applying parallel laser processing on PCB composites [10].

In the present study, the potential of laser ablation for inhomogeneous material by choosing a defined laser tilt angle is investigated.

Nomenclature

P_{av}	average power
v_{scan}	scan speed
Δs	pulse to pulse distance in scan direction
Δl	hatch distance
$\Delta l'$	projected hatch distance
F	pulse fluence
n	number of layers
θ	tilt angle
E_p	pulse energy
f_{rep}	repetition rate
ω_0	beam waist radius
ω_0'	projected beam waist radius

2. Experimental

Laser treatment is applied on the sidewalls of additive manufactured nickel-base alloy samples. The size of the samples is 10 x 10 x 10 mm³. The composition of the powder used for the selective laser melting process is listed in table 1.

Table 1. Chemical composition of CM247LC (wt%).

C	Cr	Co	W	Mo	Ta	Al	Ti	Hf	B	Zr	Ni
0.06	8.4	9.4	9.6	0.5	3.3	5.6	0.8	1.4	0.01	0.09	60.84

A solid-state laser with the pulse width of 10 ps is used to reduce the surface roughness of the samples. The beam was focused by an f-theta lens with a focal length of 160 mm. The beam radius was measured using a commercial beam camera from Ophir, see Fig. 1a. The beam radius determined in the focal plane is ω_0 = 25.4 µm. The change of the beam radius along the beam propagation axis and the corresponding change of pulse fluence is shown in Fig. 1b.

a)

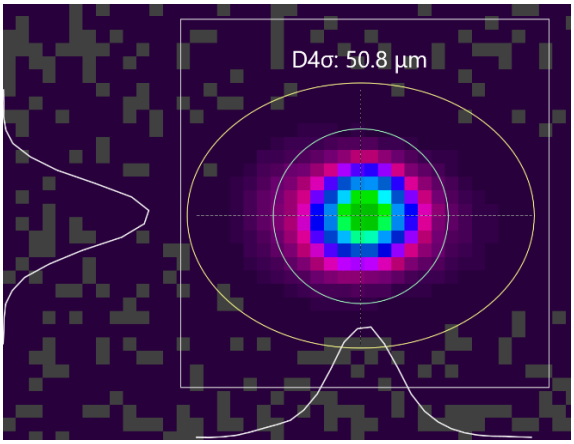

b)

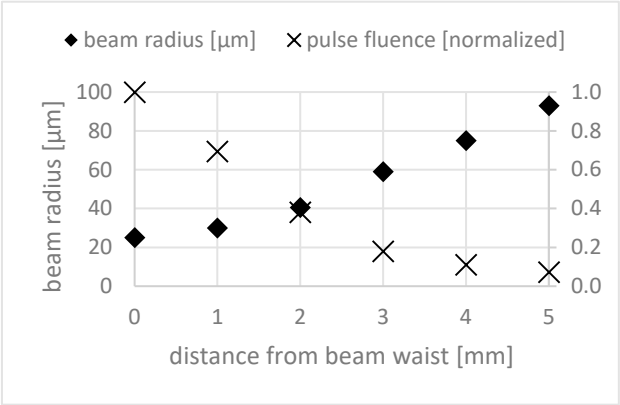

Fig. 1. (a) beam profile in the focal plane; (b) beam radius measured at different positions along the beam propagation axis and corresponding pulse fluence.

In a pre-study, the resulting angle for a standard orthogonal processing strategy is studied. Therefore, pockets with the area of 3 x 3 mm² are ablated. A unidirectional scanning strategy with 0°/90° orientation according to Fig 2 is applied. The pulse fluence F is calculated according to equation (1). The laser parameters are listed in table 2.

$$F = \frac{E_p}{{\omega_0}^2 \cdot \pi} \quad (1)$$

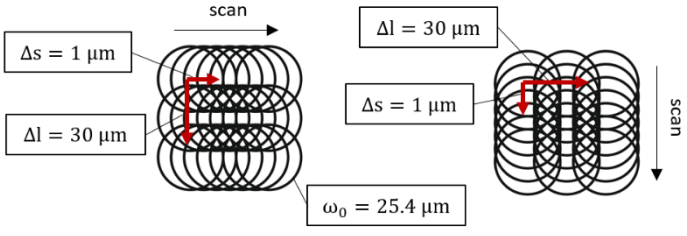

Fig. 2. Schematic distribution of the laser pulses on the sample for the pre-experiment.

Table 2: laser process parameters for the pre-study.

P_{av}	f_{rep}	v_{scan}	Δl	E_p	F	n
3 W	500 kHz	0.5 m s^{-1}	30 µm	6 µJ	0.3 J cm^{-2}	5000

Optical and confocal microscopy is used for analyzing the ablated pocket. The surface roughness measurement is performed according to ISO 25178 using confocal microscopy.

The Ni-base sample is tilted by a tilt angle θ for the surface flattening experiment parallel or orthogonal to the layer orientation, see Fig. 3. The projected pulse fluence F(θ) is calculated according to equation (2).

$$F(\theta) = \frac{E_p \cdot \cos(\theta)}{\omega_0^2 \cdot \pi} \quad (2)$$

3. Results and Discussion

The pocket for the pre-study is ablated according to the parameters mentioned in the previous section. Formation of debris next to the ablated pocket can be recognized in Fig. 3a. The bottom of the ablated pocket exhibits irregular topography. Exposure of sharp spikes can be observed in the 3D view in Fig. 4c. The size and position of the spikes are stochastically distributed. This result most likely is caused by the grain structure in the Ni-base alloy material. However, the surface at the sidewall reveals a flat surface topography. Small valleys in a constant distance are visible on the sidewall in Fig. 4c. They most likely derive from the scanning strategy.

The angle of the sidewall is determined by measuring the taper angle at 20 positions parallel and orthogonal to the layer orientation of the SLM process, see Fig. 4a. The average sidewall angle in parallel orientation is about 75° within a range of +8° and -5°. Orthogonal to the SLM layer orientation, the average angle is about 80° within a range of +6° and -6°. A steeper sidewall angle is observed perpendicular to the SLM layer orientation, see Fig. 4a,4b.

The flattening experiment is performed at parallel and orthogonal orientation of the SLM layers towards the laser beam, see Fig. 2. The tilt angle is varied between 75° and 80° in order to study its influence on the surface topography. The surface roughness before the treatment is Sa = 14.4 µm.

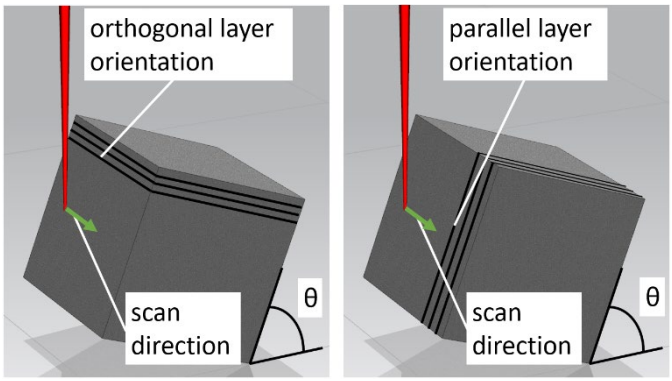

Fig. 3. Schematic illustration of the two different sample orientations for the surface flattening experiment.

a), b)

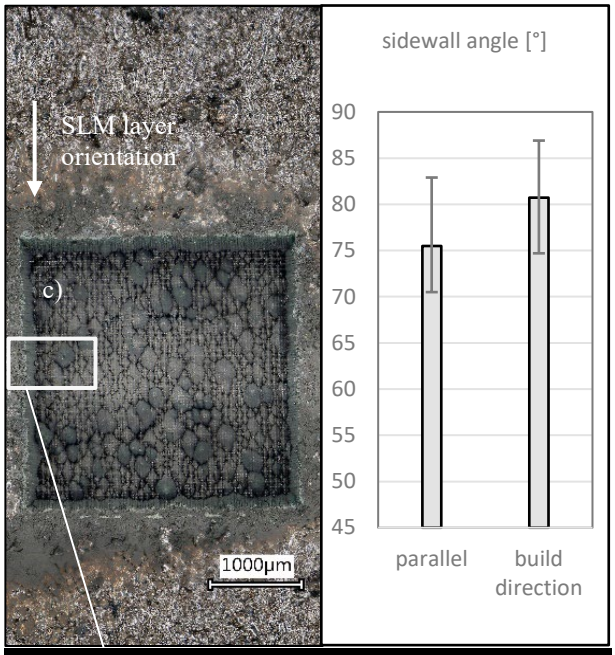

c)

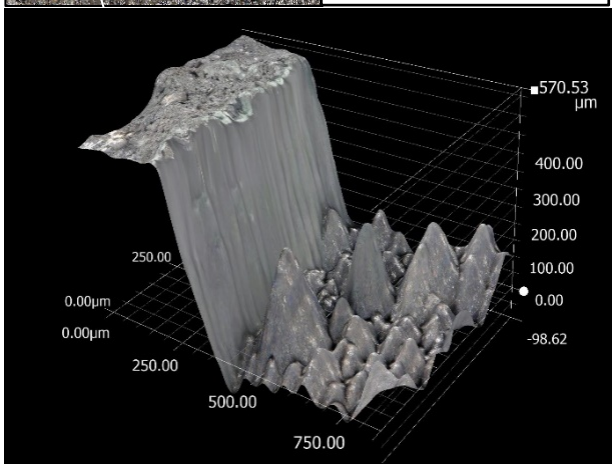

Fig. 4. Analysis of the pre-study (a) image of the ablated pocket; (b) sidewall angle measurement result, (c) 3D plot from the ablated pocket.

The scan strategy is the same like in the pre-study, listed in in table 2. The number of repetitions is reduced to n = 1000. Due to the tilt angle applied, this scan strategy leads to a different projection of the laser pulses on the surface of the sample. The projected hatch distance $\Delta l' = 172.8\,\mu m$ and the projected pulse to pulse distance in scan direction $\Delta s = 5.8$ µm for atilt angle of $\theta = 80°$ are illustrated in Fig. 5. The pulse energy is varied between 12 µJ and 36 µJ to investigate its influence on the surface roughness. The resulting projected pulse fluence is calculated according to equation (2), see table 3.

Table 3: Projected fluence for different parameters applied

E_p [µJ]	12	24	36	12	24	36
θ [°]		75			80	
F(θ) [J cm^{-2}]	0.16	0.32	0.47	0.11	0.21	0.32

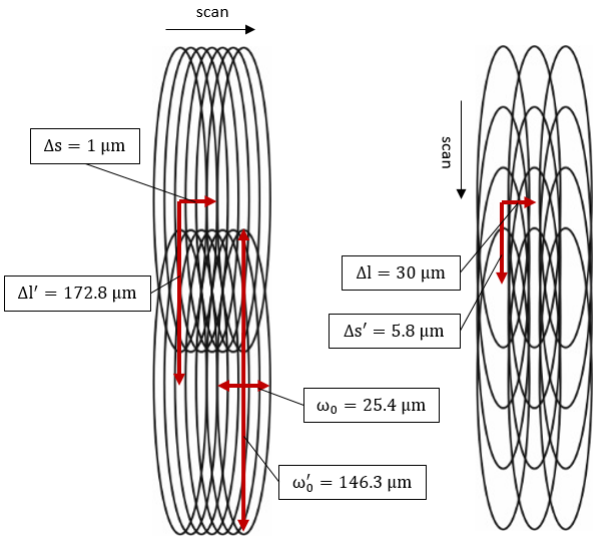

Fig. 5. Schematic distribution of the laser spots for the 0° (left) /90° (right) scanning strategy at a tilt angle of 80°.

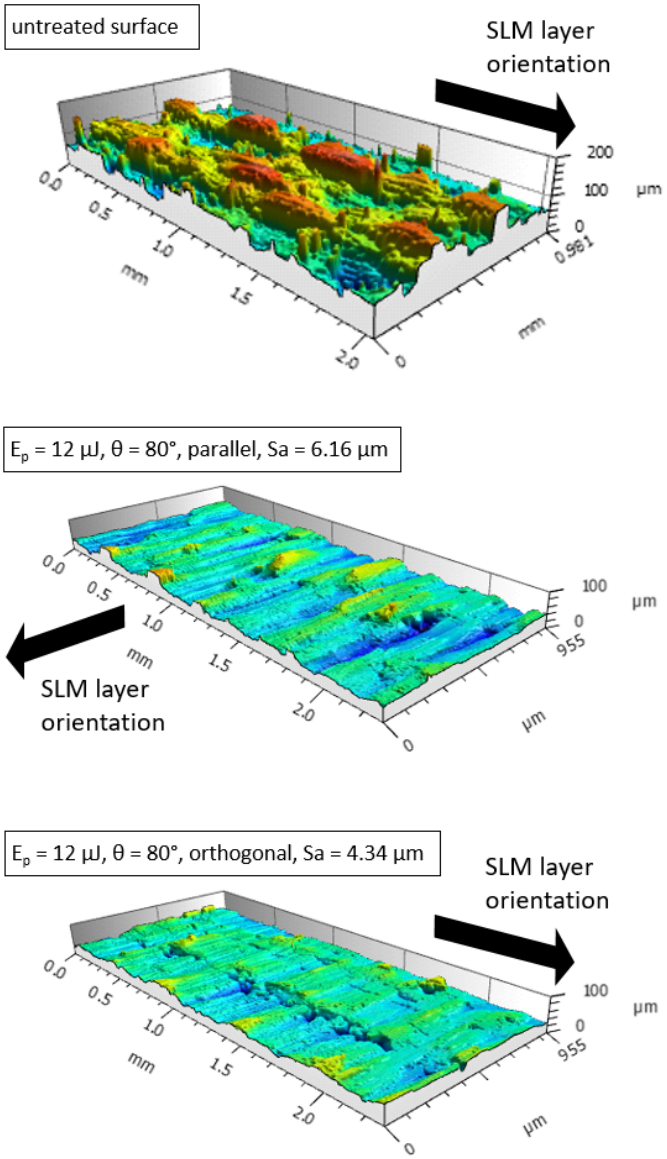

Fig. 6. Topography of the substrate after laser treatment with the same parameters but different layer orientation.

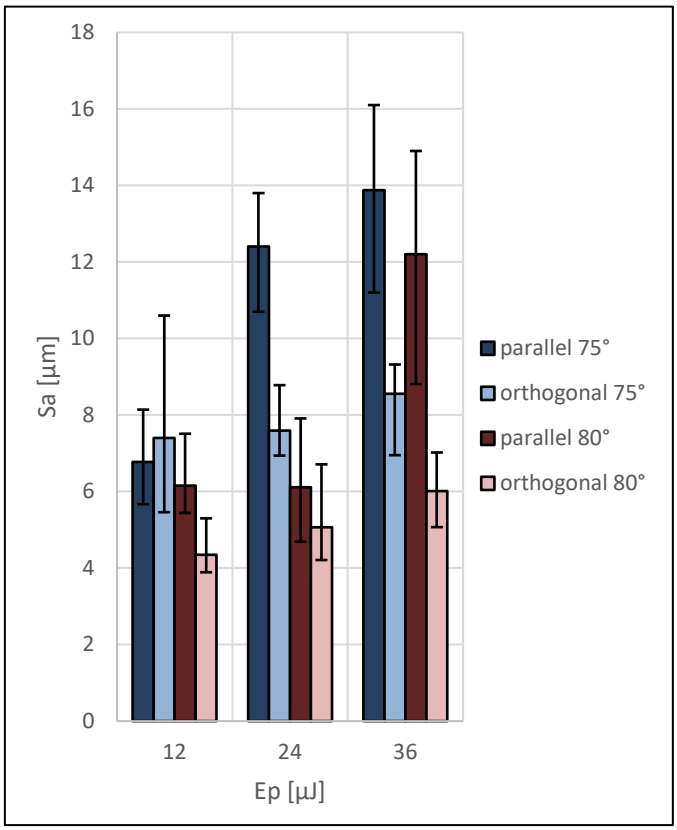

Fig. 7. Plot of the measured Sa values as a function of the pulse energy.

The Sa values measured for each parameter configuration are correlated to the pulse energy, see Fig. 7. The lowest Sa value by laser ablation is achieved at orthogonal orientation of the SLM layers, a tilt angle of 80° and a pulse energy $E_p = 12$ µJ. For the parallel orientation of the SLM layers, the lowest value $S_a = 6.11$ µm is achieved at a tilt angle of 80° and a pulse energy $E_p = 24$ µJ. The highest pulse energy of 36 µJ leads to higher surface roughness for all parameter configurations. For this pulse energy the highest surface roughness resulted for the parallel orientation at a tilt angle $\theta = 75°$ which results in a higher pulse fluence compared to the configuration $\theta = 75°$. It can be derived, that the resulting surface roughness is more sensitive to the pulse energy applied at parallel orientation.

In Fig. 6 the topography of two samples, processed with the same scan strategy and the same laser parameters with different layer-orientation towards the laser beam are compared. The corresponding pulse distribution is illustrated in Fig. 5. The sample processed at the parallel orientation exhibits high roughness perpendicular to the orientation of the SLM layers and the laser beam. An orientation of the roughness is visible. The sample processed at orthogonal orientation exhibits roughness perpendicular to the laser beam as well. This indicates that the scanning strategy is influencing the surface topography but on a lower scale. This corresponds to the topography of the sidewalls analyzed in the pre-study.

The orientation of the SLM layers towards the laser beam has an influence on the resulting surface topography. The roughness isotropy is higher for the orthogonal orientation.

4. Conclusion

Ni- base alloys manufactured by SLM are ablated by 10 ps Nd:YAG laser at different pulse energy and different tilt angle. Orthogonal laser ablation of multiple layers leads to high surface roughness. It is not possible to achieve a flattening effect on Ni-base alloy samples by orthogonal laser scanning strategy with the laser parameters applied. The ablated surface exhibits irregular surface topography due to the inhomogeneous material composition. Sharp spikes with a stochastic size-distribution are observed.

Surface flattening is demonstrated by applying a suitable tilt angle. The required tilt angle is determined in a pre-experiment by measuring the angle of the sidewalls in the ablation pockets after orthogonal ablation. This angle is transferred as tilt angle to the surface flattening experiment. Applying a tilt angle of 75° and 80° in combination with a projected pulse fluence in the range between 0.11 J cm^{-2} and 0.47 J cm^{-2} leads to surface flattening.

The influence of the SLM layer orientation parallel or orthogonal to the incident beam is studied. For parallel orientation the measurements reveal limited flattening effect of the SLM layers as well as higher sensitivity of the surface roughness on the pulse energy applied. The surface roughness Sa is reduced by more than a factor of three at orthogonal orientation of the SLM layers by a tilt angle of 80° and a pulse energy of 12 µJ which corresponds to a projected pulse fluence of 0.11 J cm^{-2}.

It is pointed out that the flattening mechanism does not require a melting phase in contrast to classical laser polishing approaches [11]. This minimizes the heat conduction into the residual bulk material. In further research, the combination of different flattening approaches should be investigated in order to further reduce the surface roughness. In order to scale up the flattening rate, different scan strategies as well as beam shaping possibilities should be evaluated.

Acknowledgements

The authors wish to gratefully acknowledge the technical support provided by the Institute of Machine Tools and Manufacturing and the inspire AG (Zürich, CH).

References

[1] Chichkov, B.N., Momma, C., Nolte, S., Von Alvensleben, F., Tünnermann, A., 1996. Femtosecond, picosecond and nanosecond laser ablation of solids, Applied Physics A 63(2), p. 109-115.
[2] Harris, K., Erickson, G. L., Schwer, R. E., 1984. MAR M 247 derivations—CM 247 LC DS alloy, CMSX® single crystal alloys, properties and performance, 5th Int. Symp; p. 221-230.
[3] Davis, J. R., 2010. Nickel, cobalt, and their alloys, ASM international.
[4] Soares, C., 2011. Gas turbines: a handbook of air, land and sea applications, Elsevier.
[5] Carter, L. N., Attallah, M. M., Reed, R., C., 2012. Laser powder bed fabrication of nickel-base superalloys: influence of parameters; characterisation, quantification and mitigation of cracking, Superalloys, p. 577-586.
[6] Krewinkel, R., A., 2013. Review of gas turbine effusion cooling studies, International Journal of Heat and Mass Transfer 66, p. 706-722.
[7] Snyder, J., C., 2019. Thole KA. Effect of Additive Manufacturing Process Parameters on Turbine Cooling, ASME Turbo Expo 2019: Turbomachinery Technical Conference and Exposition 2019.
[8] Dos Santos Solheid, J., Seifert, H., J., Pfleging, W., 2018. Laser surface modification and polishing of additive manufactured metallic parts, Procedia CIRP 74, p. 280-284.
[9] Romoli, L., 2018. Flattening of surface roughness in ultrashort pulsed laser micro-milling, Precision Engineering 51, p. 331-337.
[10] Timmer, J., H., 2001. Laserkonditionnieren von CBN- und Diamantschleifscheiben, Vulkan, Essen.
[11] Perry, T., L., Werschmoeller, D., Li, X., Pfefferkorn, F., E., Duffie, N., A., 2009. The effect of laser pulse duration and feed rate on pulsed laser polishing of microfabricated nickel samples, Journal of Manufacturing Science and Engineering 131(3), p. 031002.